Contribution To The Numerical Investigation Of The Internal cooling of An Innovative Trailing Edge Geometry Of A Turbine Blade: Stationary And Rotating Conditions.

A. Beniaiche [1], C. Carcasci[2], B. Facchini[2]

[1] Laboratory of Thermal Power Systems, Ecole Militaire Polytechnique, EMP BP17 Bordj El Bahri, 16046, Algiers, Algeria.

[2] DIEF: Department of Industrial Engineering, University of Florence, Florence, Italy.

[2]Correspondence author: A. BeniaicheFax: +213661813532 Email: beniaiche_ahmed25@yahoo.fr

ABSTRACT

In this paper, a numerical aero-thermal validation has been carried out for two (02) 30:1 scaled models with ribbed internal surface representing a geometry of an original trailing edge (TE) composed of single row of seven enlarged pedestals in immobile and turning conditions for high Reynolds numbers. The commercial ANSYS-Fluent software is used to perform a CFD analysis modeling the isothermal air flow inside the stationary geometry by means of the k-ω SST turbulence model. PIV in addition to TLC experimental data were employed to verify the numerical model aero-thermally; qualitatively and quantitatively for different working conditions (Re = 10000-40000 and Ro = 0-0.23), respectively. Numerical results reveal, under rotating conditions, a disappearance of the observed horse-shoe structures of the stationary conditions inside the TE exit region, a decrease of the flow approaching angle and an acceleration of its velocity beside a surplus calculation of the turbulence Kinetic Energy (k). The obtained results, during the design process, assist the understanding and the forecast of the flow field behavior by the assessment of the aerodynamic and thermal performances of the considered blade cooling geometry.

KEYWORDS: CFD ; TLC ; PIV ; Trailing edge ; blade cooling system ; Heat transfer ; Pedestal ; Heat transfer coefficient ; Nusselt Number.

Nomenclature

A xy	Plane [--]
B xy	Plane [--]
$Cxyz$	Velocity magnitude in planes xyz [m/s]
D_h	Hydraulic diameter [mm]
D	Distance from pedestal's leading edge to inlet section [mm]
HTC	Heat transfer coefficient [$W\,m^{-2}K^{-1}$]
H_1	Initial duct height [mm]
U_b	Bulk velocity defined at the inlet section [ms^{-1}]
u	x velocity component [ms^{-1}]
u', v', w'	Fluctuations of the x, y and z velocities components [ms^{-1}]
V	y velocity component [ms^{-1}]
W	Axial velocity component [ms^{-1}]
N	The total number of cells
Nu	Averaged Nusselt number [--]
P_x	Pitch inter-pedestals distance [mm]
$\dot{Q}$	Heat flux rate [W/m^2]
Re	Reynolds number [--]
Ro	Local rotation number[--]
x	Radial direction [--]
xy	Plane xy
xz	Plane xz
y	Rotation axis direction [--]
y/D	Dimensionless distance [--]
yz	Plane yz
y^+	Dimensionless wall distance[--]

y/P_x	Dimensionless position [--]
z	Axial direction [--]
z/D	Dimensionless [--]

Greeks

α	Wedge angle of the inclined wall or angle of attack [°].
γ	Model inclination angle [°]

Acronyms

AR	Aspect Ratio
HTC	Heat transfer coefficient
LE	Leading Edge
L0	Trailing edge central region
*L*1	Trailing edge pedestalsregion
PIV	Particles Infrared Velocimetry
PMMA	Poly Methyl Methacrylate
PS	Pressure side
TLC	Thermochromic Liquid Crystal
SS	Suction side

Subscripts

avg	Average
max	Maximum
meanX	Corresponds to the mean *x* line
meanY	Correspond to the mean *y* line
meanZ	Correspond to the mean *z* line

Introduction

All over the most recent times, the fashionable manufacturing of powerful engines with best efficiency became possible thanks to the boost of the turbine inlet temperature (TIT), and the use of efficient cooling systems, especially those located at the thin trailing edges (TE) [1]. In fact, the TE of the blade is the most critical [2] because of the colossal thermal and structural

tensions which it faces. The proposed contemporary design solutions to cool the thin trailing edges are based on shapes set among pedestals, so as to raising the internal heat exchange [3] and reducing both the weight and the aero thermal stresses. For that reason, and in order to optimize: the coolant, the internal surfaces and the life span of the blade, it is critical to improve the comprehend about the local heat exchange at this area.

The open technical literature offers a series of experimental and numerical studies dealing with the employ of different perurbators; such as: pedestals, pin fins of diverse shape and configuration, affecting the studied phenomenon. For instance, Metzger and Haley [4] and Metzger and al. [5, 6] published an experimental study of the effect of increasing the flow speed on both the pressure losses and the heat transfer within specific trailing edge shapes by means of enlarged pedestals and pin fins inside a converging canal. Wang et al. [7, 8] presented a notable experimental work as a result of their full heat transfer assessment on end-wall plane mounted of a range of pedestals. Works of Taslim et al. [9, 10] are experimental and numerical contributions showing the jet impingement effects in a conduit with an axial outflow. Later, Hwang and Lui [11, 12] presented an evaluation of the pressure losses and the heat transfer in cool geometries of typical authentic blades trailing edge parts (pin form and wedge and trapezoidal channels). They avowed that the fluid flow in rotating blade cooling channels is significantly affected by Coriolis and centrifugal forces. Not long, Facchini et al. [13] carried out an experimental study in a converging duct using enlarged pedestals and pin fins of circular form. They demonstrated that both the heat transfer and pressure losses are affected positively by acceleration of flow.

Chang and Liu [14], or Holes Rallabandi et al. [15] studied the thermal field searches inside a turning a trapezoidal cross-section channel. The flow discharge is insured via holes at the TE. Authors proposed correlations ready-to-use and valid as well for rotation complex geometries models.

Regarding pin arrays performances, just only some efforts focused on the mixed axial-radial inflow effect conditions such as works of Kulasekharan and Prasad [16] and by Bianchini et al. [17, 18] who revealed the visible consequence of the use of combined orientation (axial –radial) on the heat exchange. Afterward, Armellini et al. [19] used detailed PIV and stereo-PIV measurements in a model scaled to 30:1 reproducing internal cooling ducts in motionless and orthogonally rotating working conditions to study the flow field of

the present cooling channel geometry. Results revealed that the Coriolis altered considerably the flow field upstream of the pedestals. Later, Bonanni et al. [20] used the same TE of [19] to measure experimentally effects of the rotation on the heat transfer with smooth, +60 ribs and -60 ribs, for a Re = 20000 and a Ro = 0 - 0.3. Results revealed that the high peaks of HTC are seen to shrink with the increase of Ro number.

Hart et al. [21] and Speziale et al. [22, 23] presented the main contributions analysing the fundamental pattern of a radial passage with rectangular cross-section rotating orthogonally. The main result of the experimental survey by Johnston et al. [24] was the intensification turbulent stresses by sensible spanwise rotations on the so-labeled unstable and stable channel sides. Wu et al. [25] performed experimentation of a complete trailing edge cavity reproducing a original internal cooling channels turbine's blade to evaluate the heat transfer and pressure drop, at a high Reynolds number (20000 – 50000). They used the TLC technique to measure the local heat transfer on both pressure and suction sides. In the case with bleed flow, on suction side, results showed that, in the first and second channels, the local heat transfer is less than on pressure side, while with no bleed flow, local heat transfer increased notably on the pressure side in the first and third channels at the same time as it is lower on the suction side.

A complete experimental analysis was conducted by Coletti et al. [27] on internal cooling geometry comparable to the one used by [9]. Later, the same authors studied the turbulent flows inside a channel supplied by crossways ribs along one wall under rotating conditions [26] through 2D time-resolved particle image velocimetry. They performed their experimentations for Re = 15 000 and a Ro = 0.38. Results highlighted the impact of the rotational buoyancy on the flow.

The improvement of the contemporary CFD tools allowed an improved understanding of the studied cooling channels phenomenon's illustrated by varying the cross-section profiles and design. The works of Donahoo et al. [28], Ooi et al. [29] and Luo et al. [30], Viswanathan and Tafti [31], and Spring et al. [32] are examples of cooling channels of nozzle blades simulations, in stationary setting. In fact, Saha and Acharya [33] used LES simulation and the k-ε turbulence model to carry out a wide unsteady study, for affirmation reason, on a square pin array. Afterward, Delibra et al. [34] analyzed the heat transfer and flow field, by means of CFD tools, around eight circular pins composing a periodic array.

They gave also partial heat transfer predictions results. However, the effect of variable cross section ducts was analyzed by Di Carmine et al. [35] who were interested into the performances survey of pin arrays. In the open literature, no work can be found considering the rotation's effect on wedge shaped channels with a combined axial-radial flow. Schuler et al.[36], Prakash and Zerkle [37], and Tafti and Elyyan [38] investigated the rotation conditions effects on typical turbulators for dimples where the turbulence promoters; similar to enlarged pedestals. The investigation of the thermal performances modification due the aspect ratio of the cross-section effect, in a rectangular smooth and ribbed channel, was performed by Saha and Acharya [39], via an unsteady RANS resolution.

Soon after, Andrei et al. [40] provided a CFD examination of the heat transfer in a trailing edge cooling channel. static and rotary condition were considered for k −ω SST RANS model using a structured multi-blocks mesh for the Open Foam and CFX codes. Their conclusions were that the Open Foam code results excel those of CFX code. Soon after, the same geometry studied by [18, 19, 20 and 42] was investigated in term of the aerodynamic flow field behavior by Pascotto et al. [41] via RANS and 8 10^6 hexahedral nodes model for a Re = 20000, and Ro = [0, 0.23, 0.46]. They chose three orientations: 0°, 22.5° and 45° for the channel, expanding preceding results to new engine-like working conditions. PIV data were used to validate the numerical ones.

In recent times, Beniaiche et al. [42] performed an experimental analysis on the same geometry used by authors of [18, 19, 20, 40 and 41], for +60° ribbed geometry, via complete TLC measurements. The Reynolds number was in range of 10000-40000 and a Rotation number up to 0.15. They concluded that *Re, Pr, Ro* and *Xr* all affect the heat transfer coefficient.

Later, Beniaiche et al. presented, respectively, two complementary studies dealing with the experimental [43] and the a numerical simulation [44] of the same geometry studied by [20 and 42] but only for a smooth geometry for Re= 10000 to 40000 and Ro up to 0,23 by still focusing on the trailing edge exit area. Authors showed that, also as it was for ribbed surfaces [42], the flow operating conditions and the position of the inter-pedestal's region have a serious effect on the heat transfer echange; which allowed them to propose correlations based on those parameters. The agreement between the numerical results and those of the PIV and TLC techniques data was considered very satisfying after comparison to the PIV and TLC

data. The numerical model revealed the existence of horse-shoe structures at the inter-pedestals regions affecting the heat transfer performance. These structures, known to be difficult to be explored by mean of experimentation, are also affected by the increase of the rotation number. These aerodynamic insights enhance the understanding and explanation of the obtained thermal data of [43].

This paper is a complementary work of the experimental one started by authors in [42], aiming to extend the understanding of the prior experimental results thanks to the numerical data allowing to reveal the aero-thermal behavior features of the flow cooling, usually not easy to be attained experimentally with no altering of flow. Therefore, this work aims not to assess the potential of the numerical solver but to deep understand the reasons behind the modification in the flow field and heat exchange when the operating conditions change; especially the Reynolds number and the Rotation number; in order to enrich the comprehension of the studied phenomenon by the only some works available on this topic.

1. Definition of the studied geometry

Authors conducted the experimental procedure at the Department of Industrial Engineering, University of Florence, Florence. At the trailing edge, the ejection channel region is a wedge shaped and contains a row of (07) enlarged pedestals (figure 1.a). Detailed dimensions are reported on figure 1a, 1b, 1c and 1d. The characteristics of the studied geometries and the operating conditions are resumed in table 1.

The used channel is split in two parts: the L0 and the L1 region (figures 1a, 1.b and 1.c). It steer the flow from the radial inlet to the tangential outlet. The L0 region is a constant height conduit with inclined lateral wall used both to diminish the passage region along the radial direction and redirect the coolant in the direction of the trailing edge exit. However, L1 is the region where the pedestals are positioned. The Nusselt number data will be collected at each inter pedestals region, as it was the case for the experimental procedure. For further information regarding the experimental procedure and its data reduction, please refer to our works [42, 43].

1.1 Numerical approach

The used mesh is a structured multi-block (figure 2) made of 9.5 10^6 hexahedral cells forms the computational domain. In order to reproduce the flow separations taking place in the regions approximately the pedestal surfaces [20, 43 and 44], the need of very fine elements justified this high number of cells. Also, high orthogonally cells are obtained by the use of O-grids [41]. The solver ANSYS-Fluent 14.0 was used to perform the CFD calculations. As it was for [44], the Navier-Stokes equations are solved using a SIMPLE-like (Semi-Implicit Method for Pressure-Linked Equations) algorithm with a convective diffusive equation for the pressure correction to impose mass continuity considering density variation. Convective schemes uses a second order upwind interpolation scheme based on the NVA (normalized variable approach) known in the literature as self-filtered centered difference [44] blended with a deferred approach with a first order upwind scheme. Turbulence was modeled by means of k − ω SST model with a hybrid near wall treatment, because it has been proved to predict reasonably well the flows inside rotating channels [44].

The Reynolds number is chosen to be 20000 and 40000. The calculation of this parameter is referred to the inlet hydraulic diameter D_h.

An adiabatic conditions and no slip is imposed on viscous walls. Only one surface is heated (see figure 1) where a constant heat flux ($\dot{Q}$= 1500 W/m^2) was applied. At the inlet, an experimental velocity profile (equ: 1, figure 3 a,b), obtained by [19] and [41], was applied and at the exit an ambient static pressure, P = 101325 Pa , was retained.

$$V_{inlet}\left(\frac{x}{D_h},\frac{y}{D_h}\right)=V_{meanY}\left(\frac{x}{D_h}\right).\frac{V_{meanX}\left(\frac{y}{D_h}\right)}{V_{meanX}(0)} \qquad (1)$$

1.2 Planes definition

Figure 4 illustrates the defined planes and their positions used to carry out the analysis and comparison of the found data. Tables 2 and 3 summarize the planes locations in the x y z space.

1.2.1 Aero-dynamic results

First of all, before starting simulations, the validity of the CFD model must be verified. To reach this goal, it has been decided to confront its data to two referenced data: aerodynamic and thermal ones.

For the first validation, the aerodynamic data are those of the PIV technique experimentation provided by [19, 41, 44], at the same operating conditions of Re = 20000 and Ro = 0-0.23. However, in the second confirmation will assessed by means of 2D HTC maps experimental data obtained by authors thanks to TLC experimentation, for ribbed surfaces, for closed and open tip configurations, at Re = 20000-40000, and Ro = 0-0.23.

The calculation of discretization error of the computed results must be evaluated. This step is possible thanks to the recommended well-established method of the Fluid Engineering Division of ASME [44, 45] allows a fulfillment of the grid independence revision. This method, as applied to a wide range of CFD problems, is based on a generalized formulation of the Richardson extrapolation theory [46, 44] proposed by Roache [44, 47, 48] to compute the called “grid convergence index” (GCI) which represents the discretization error bands for the computed variable [44].

In our case, and as authors did in [44]; three similar grids were set using a refinement factor of 2.2 to diverse the spatial resolution. The GCI method was applied to insure the homogeneity of refinement factor all along the three spatial directions, and to use just similar geometrical cells. The core parameters and results of the mesh sensitivity analysis are summarized in Table 1, comparing results of the CFD data and those of Pascotto et al. [41]. N, $y^{+}{}_{\max}$ and $y^{+}{}_{\text{avg}}$ represent: the total

number of cells, the maximum value of the normalized wall distance for the cells close to the walls, and the mean value of the overall mesh, for +60° ribbed surface, open tip condition, for Re = 20000 at stationary conditions, respectively [44].

Figures 5a and 5b, illustrate the CFD profile of the velocity modulus, C_{xyz} , at two positions: $y = -132$ mm along z and x directions, respectively, compared to Pascottto et al.[41] results. On figure 6b, only the GCI of the present study is presented for precision. As a remark, a good conformity is found among results of the two numerical studies. The local value of the GCI is represented by each error bar, calculated for the finest mesh, in the z and x directions, respectively. The analysis confirms pleasing agreement along all the channel dimensions, for an averaged inaccuracy less than 3%. It is to notice that the limited regions contained by the boundary layers are distinguished by lesser velocity and high discrepancies, so have made an exemption to the agreement just found before [43].

Table 4 resumes data of y^+_{max} and y^+_{avg} of the present study compared to those of Pascotto et al. [41], for different mesh sizes. The discrepancies are about 3.4% for y^+_{max} and 10.9 % for y^+_{avg}, respectively. Indeed, $y^+<1$ assures the correct near-wall integration for both stationary and rotating conditions. To respect this condition, on all the viscous surfaces, the thermal boundary layer is decomposed of 20 elements. A constant heat flux of 1500 W/m^2 is applied to the bottom surface, using different tip conditions: closed tip and open tip. An illustration of the obtained y^+ distribution is given on Figure 6, using the fine mesh, along the heated surface, for open tip (Figure 6a) and closed tip (figure 6b) conditions, respectively.

To well verify the robustness of the present CFD model, the validation of its results under rotating conditions is necessary. A good conformity is found on figure 7 showing the V/U_b ratio (the mean velocity component/the bulk flow velocity), at $x = -69.8$ mm position of the inlet channel, in the symmetry planes, for Re = 20000 at Ro = 0 (Figure 7a), and Ro =0.23 (Figure 7b). It is clear that, at the leading edge, the trivial flow disproportion in the direction of the TE side of the conduit ($y< 0$) is well

reproduced for Ro = 0 (Figure 7a) due to the blockage effect imposed by the redirecting wall. Also, under rotating conditions (figure 7b), the CFD computations reproduce well the sturdy flow imbalance in the direction of the leading side (y > 0) which is in opposition to the one observed (figure 7a) because of effects of the potential flow. In fact, the faintly viscous flow inflowing the channel tries to preserve its angular momentum which increases the relative eddies having an opposite angular velocity direction to the rotating channel's one. So, the counter-rotating eddies is superposed to the through flow which leads to boosting the relative velocities towards the channel leading side zone and reduce in the trailing side zone.

Another parameter has been verified, in addition to the mean velocity profiles, which was the turbulence intensity I, illustrated in figure 7c for plane *xy* at *z = 0*. The experimental data were calculated using the velocities fluctuations $I = \sqrt{(u'2 + v'2 + w'2)/3}/U_{b,}$ estimated at x, y and z directions. In the present case, the experimental I is about 3, 28 [%] at the same time as calculations of the CFD turbulence intensity (figure 7c) was obtained thanks to the *Turbulence Kinetic Energy k* and defined by equation 2:

$$I = \sqrt{2/3.k}/U_b = 2.86\%. \quad (2)$$

Continuing more evaluating the CFD-code results, and for a better comprehension of the studied phenomenon, it is useful to check both local velocities profiles and HTC data. For that reason, it was decided to compare first the numerical flow velocity profiles to those of PIV experimentation and later the CFD HTC 2D map to those obtained experimentally by means of TLC technique.

On Figure 8, it can be seen a comparison of the C_{xz}/U_b velocity ratio profile distribution, for an open tip geometry for Re=20000: figure (8a,c) presents the experimental PIV data [Pascotto el al.] and (8b,d) those of the CFD prediction, for stationary (Ro = 0, figure 8(a,b)) and rotation condition (Ro = 0.23, figure 8(c,d)),

respectively. Generally speaking, the CFD simulation is capable to reproduce both the major flow characteristics and the profiles velocity distribution as well their modification due to rotation effect as it is illustrated by the correct prediction of a larger recirculation region at the channel tip. However, it has to be noted that larger recirculation is always predicted in both static and rotating conditions, but this discrepancy is considered to be of minor importance in view of the scope of the present contribution. It can be observed that the amendment of the flow characteristics and velocity distribution by reason of rotation effect were well imitated, as it is demonstrated by the acceptable prediction of the recirculation zone at the tip region. In fact, compared to static conditions, in the mean flow at upper radii, Coriolis effects turning out are further powerful, as shown by both experimental figure 8(c) and numerical figure 8(d) results. By comparing Figures 8(a,b), diverse flow paths can be viewed compared to Figures 8(c,d). In plane *xy*, the Coriolis force is acting along the normal direction to the stream-tracers plane following $y < 0$, and is proportional to the in-plane flow velocity modulus *Cxy*. Therefore, on the core flow the Coriolis force is seen to be stronger, which consequences a considerable change, at different channel elevations, of the curvature of the stream-tracers. Also, the intensity of the core flow redirection towards the TE exit is seen to be reduced, due to the thinning of boundary layer flow near the upper and the down walls, due to its higher inertia [43]. Definitely, this work aims to study the field under the rotation effect with respect to the flow characteristics which may affect the heat exchange performance. From this view-point, a satisfactory accuracy of the predictions is realized; indeed the numerical too is able to capture the existence/absence of these aerodynamic features and their changes, for different working conditions.

1.2.3 Thermal results

The experimental TLC data provided full 2D HTC maps distribution over the heated surface. In order to ensure an easy assessment and understandings of the obtained results, the identical color range and level scale is applied to plots of HTC 2D maps. The x/P_x is a dimensionless distance with the origin is located on the mid-span of the L1 region, and y/D is a dimensionless distance with the origin is the right plan of the inlet section [19, 20, 43 and 42]. (see Figure 1a). [43]

Figure 9 and 10 illustrate results related to stationary and rotation (Ro = 0.23) conditions, respectively, of a ribbed +60° surface for Re = 20000 and Re = 40000. A good qualitative agreement is found between experimental and numerical results. It is clear, on figure 9, that the shrinkage of the flow passage area induces an acceleration of the coolant velocity, in region L0, and as soon as the coolant arrives at the ribs close to the redirecting wall, the ribs alters its movement and the turbulence disorder augments, and because of the orientation of ribs, the flow is oriented on the way to the inclined wall, and which enhances the turbulence disturbance much more. Moreover, as moving forward the tip, the efficiency of the cooling decreases because of the increase of bulk temperature. Furthermore, recirculating flow regions near the rib (figure 11) are more distinguished by a significant 3D structure near to the inclined wall plus to overall flow deviation towards TE exit. Consequently, CFD thermal HTC data (figure 9) have a larger extension downstream rib, and higher HTC peaks in the proximity of the impingement of the flow near the inclined wall. A lower HTC values are noticed between the reattachment position and the next rib.

The effect of rotation on the increase of the heat exchanges is given on figure 9. In fact, both the increase of Re and Ro raise the HTC values compared to those of figure 10, for the same Reynolds number working conditions (Figures 9a,c/ 10a,c) and (Figures 9b,d/ 10b,d). The explanation of these increases might be supported by the analysis of the coolant local efficiency through the radial direction. For that reason, figure 11 demonstrates an assessment of numerical data to those of

experimentation of the averaged reduction of coolant temperature potential along the position, (x = z = 0), for stationary and rotating conditions, at each slot of the line y/D = 4, using an open tip configuration, for Re = 20000. Equation (3) defines the coolant temperature potential as follows [44, 47, Beniaiche et al 2]:

$$\frac{(T_b - T_w)}{(T_{co} - T_w)} = \text{The efficiency of the coolent temperature potential} \quad (3)$$

In fact, the local efficiency at each point of the line y/D = 4 is averaged as the sum of all the local points of the given slot divided by the number of these points. T_b is the bulk temperature, T_{co} is the temperature of the coolant at the inlet section and T_w is the wall temperature.

It is clear that the CFD prediction's data predict well the experimentation ones, with an error of about 5% to 6% for the stationary and rotating conditions, respectively.

Figure 11 highlights the reduction of the efficiency as much as the coolant goes forwards the tip region due to the fact that the main flow interacts with the heated surface and ribs. This interaction induces an increase of the bulk temperature which reduces the efficiency of the heat exchanges.

In fact, when the Coriolis force acts, it alters the flow field: the flow coolant's high momentum core is driven by the secondary flows in the direction of the heated plate; also the free shear layer created by the rib (obstacle) will have a distortion of its stability, which leads to a decreasing the length of the reattachment point along the heated surface. Figure 12 shows the comparison between the experimental (left) and the predicted (right) turbulence kinetic energy (k) between the 3rd and the 4th rib in plane xz, y = 0 mm. Besides, the experimental results [56] are used to highlight the different recirculation zones dimensions. The fluid layers adjacent to the ribbed wall are heated up and centripetal buoyancy drive them upstream. The reverse flow intermingled with the core streams on top of the ribs, which generates the called

“buoyant mixing layer”. Concerning the numerical prediction (figure 12 right), and because that the reverse flow spanning a larger floor between ribs, the mixing layer is bowed in the direction of the heated surface at $B/h_{rib} = 8.69$. Approaching the obstacles the stream tracers curve, overpassing both streams and forming the recalculating zone. The source point at the center of the recirculation highlights the 3D character of the flow. Nevertheless, since the measured velocity field is on the symmetry plane, it is expected to capture the main dynamics in the considered configuration. It is noticed that the experimental position of the reattachment point is $B/h_{rib} = 3.55$, which leads to say that the *k-w SST* model over estimates this point due to the fact that the chosen CFD model has higher values of the kenetic energy *k.* It must be noticed that assessment of the reattachment point is defined in the position where the velocity is equal to zero along axis x. Though, the obtained results reveal that configurations with turbulator are a defy for the RANS formulations. It can be noted that a slight enhancement can be obtained by LES or DNS techniques, requiring more time to reach convergence; consequently, there is no motivation to employ these techniques. As for comparison of the flow field, downstream the rib, CFD data expects a bigger expansion of the separated flow. In fact, the amount of the introduced eddy into the domain allocates the point of the reattachment position, due to the fact that in the standard SST formulation, limiters are placed on the eddy-viscosity which produces an excessive separation scale. [pascotto]

Concerning the L1 region (pedestals exit region, figures 9 and 10), the CFD model moderately well estimates the HTC values as it is illustrated by the decrease of the low HTC zones corresponding to the recirculation zone in the downstream area of each pedestal . This remark is valid for the open tip and the closed tip configurations, with some discrepancies concerning the size of the recirculation zones at each pedestal. In fact, this size is inversely proportional to the quantity of the air passing as each inter-pedestals area. It is clear that using a closed tip configuration, much more air crosses the L1 region, which leads to decrease the size of the recirculation zones

and vice-versa; using an open tip configuration, about 12.5% less air exists from the L1 region that results into an increase of the low HTC values upstream each pedestal.

As displayed in figure 13, illustrating the profiles of the velocity and the stream-tracers distribution, in planes: *A xy* (figure 13. a,c), *B xy* (figure 13 b,d), for Re = 20000 under stationary conditions. It can be concluded that every main characteristic of the flow field is well predicted by the CFD model compared to experimental data.

The agreement between numerical and experimental data is found to be good, for the time-averaged flow field, as it is illustrated by figures 14 (a,b) which represent the flow approaching the pedestals symbolized by the incidence angle α among the flow in *xy* plane and the *y* axis for both at line *y = -132 mm* (figure 14a) and the *V/U* ratio along the same line (figure 14b) for stationary conditions.

From the tip to the hub, the α angle is decreasing according to the lessening of the recirculation zones. It is shown an alternation of sign of the incidence angle α at the 1st inter-pedestal area. This is explained by the inversion of the axial velocity due to the recirculation zone effect. The CFD model over estimates its extension [43] which explicates the HTC discrepancies between the CFD model and experimentation. From P2 to P7 the similarity of the results is very good except for P8 where an over estimation is noticed. This CFD high value of the incidence angle might be elucidated by the effect of the recirculation zone at the tip of the L0 region on the redirected flow toward the exit P8 region. Even if the recirculation zone at the tip is well captured but it is quite larger than the experimental one. the tip recirculation zone's expansion accelerates the flow in the direction of the P8 slot, and leads to the recorded discrepancy of the incidence angle in figure *14a* approaching the wall side of the P8 region *(x > 525 mm)*. The same results, as those of figure *14a*, are confirmed by the comparison of the V/U_b ratios on figure *14b*, extorted along line *y =-150 mm* from plane *xy*.

In section II.2, it has been stated that, slower boundary layer flow, inside the L0 region for the stationary conditions, is more derived towards the TE than the core

flow because of its inferior inertia, in an opposite way for the rotation conditions (0.23) characterized by the Coriolis forces inertia effect. So, it is essential to check the flow field changes under rotation conditions, at the L1 region also. For that reason, figure 15 illustrates the flow approaching the pedestals symbolized by the incidence angle α, for stationary and rotating condition (Ro =0.23). Visibly, from the tip to the hub, the rotation effect induces a decrease of the angle α. In fact, an alternation of its sign of at the 6^{th} to the 7^{th} inter-pedestals area takes a place. This inversion of the sign of the axial velocity is attributed to a recirculation zone effect. As it is shown on figure 7b, the axial velocity is increased due to the rotation effect compared to the one of stationary conditions due to the axialization of the flow.

The potential of the CFD model heftiness is fulfilled by an examination of the 3D flow structures generated within the IP passage by means of the comparison of the experimental [19] (Figure 16: a,b,c, and d) and the numerical data (figure 16: e, f, g and h) in P4 inter-pedestal region on plane *A xy* (figure 16 a,e), *B xy* (figure 16 b,f), xz1 figure 16: c,g) and *xz2* (figure 16: d,h), respectively. An additional affirmation of the good matching among experimentation and CFD data under rotating conditions is given by figure 17 which illustrates the flow field within the P4 slot: figure17 (a,d) plane : xy, z = 0 mm, 17(b,e) plane : A xy, z = 14.55 mm, 17(c,f) plane : xz 1, y = -150 mm, 17 (a, b, c) Experimental PIV, 17(d, e,f) CFD results, for: Re = 20000, for Ro = 0.23.

Concerning the stationary conditions of figure 16, both the experimental [19] and CFD data located a recirculation zone on the *A xy* plane (figure 17 a,e), at x= 300 [mm] close to the upstream face of the pedestal, implies the generation of a horse-shoe vortex branch by the interaction of two interacting boundary layers : one on the heated surface however the other one on the pedestal leading side surface. Data on plane *xz1* (figure 17 c/g) prove that horseshoe vortices exist on the pressure side (z >0 mm) and the suction side (z < 0 mm). It is a clear confirmation that the CFD model predicts well simulated phenomenon (figure 17: c,d compared to 17: g,h). For sure

that some discrepancies are found in the computed CFD values in the IP region and this might be the result of the turbulence kinetic energy *k* over estimation as it has reported before. These located recirculation zone in figures 17 (a,b/e,f) corresponds to the low HTC values region in figures 9 and 10 which explains that these regions don't get the necessary cooling effect to be well cooled.

Concerning rotation effect's results; they are presented in figure 17. In fact, the flow behavior attributed to the effects of rotation which generate a notable speeding up of the flow near walls ensuing in the tapering of the boundary layers. Consequently, the horse-shoe vortices vanish inside the flow approaching the pedestal region and, indeed, the size of secondary structures is severely influenced by the boundary layer thickness. In addition, the discharged mass flow rate at the L1 region is increased due to the increase of axial velocity as it is seen in figure 15b, under the rotation effect. Consequently, as the angle of attack on pedestals is decreased (Figure 15a), under the rotation effect, inducing a decrease of the size of the separation bubble at this side (Figure 17: a,b,d,e). It can be noted that the only dissimilarity between experimental and CFD results seen on figure 17 are those contained by the region of separated flow (at x = 225 mm, downstream the pedestal) that is judged less significant. Undeniably, the in-plane velocity modulus *Cxy,* in this flow region, is near to nil, which signifies that, the fact that experimental precision affects the stream-tracers, this makes them less vital.

To continue the quantitative assessment between the obtained CFD data and experimentation, in terms of the heat transfer changes and increase, at the 08 spots of the TE region L1, seen on figures 9 compared to stationary conditions of figure 10, a comparison between the averaged Nusselt number calculated experimentally and by CFD tools is plotted on figure 18.

A good agreement of about 88% is found illustrating that CFD model predicts well the increase of the averaged Nusselt number under the rotation condition, as the Reynolds number is varied between 10000 and 40000. in fact, the Coriolis forces acting within the L0 on the main core of the flow region affect seriously the heat

transfer efficiency at of the TE exit (the L1 region), by inducing much more flow rate, characterized by the increase of the axial velocity (Figure 15b), and the disappearance of the horse-shoe (Figure 17. c,f) because of the thinning of the boundary layers on the internal wall, which leads to enhance the efficiency of the coolant at the L1 region slots. Even thought, discrepancies remain to exist and they might be related to:

1- The CFD model hypothesis might be revised. In fact, the CFD considered the surrounding walls are adiabatic.

2- The TLC pictures post processing procedure are affected by imposing the TLC band temperatures values to the black areas on pictures (cooled or over heated) which is not always a correct supposition. In the reality, these areas might have a higher or a lower temperature values than those imposed during the post processing procedure.

3- The turbulence Kinetic Energy (k) is over-estimated by the CFD model.

1.3 Conclusions

The present study is divided in two elements: the first concerning the numerical assessment of the aerodynamic and the thermal performances of an innovative internal cooling ribbed conduit for the TE of a gas turbine blade under stationary and rotating setting. The second one provides a support to well comprehend of the experimental viewed flow field under different working conditions of the studied channel. Tests were performed for Re = 20000 and 40000, within Ro=0 and 0.23. In conclusion the analysis performed showed that:

- The CFD model was capable to reproduce well the experimental observations and quantitative data.

- Inside the channel, on the ribbed wall side, the flow redirection towards the LE arises in the flow layers; due to Coriolis forces, and as a result, the cooling is enhanced as a consequence of the augment of the turbulence effect.
- For the same Rotating number, the flow behaviour in the radial development channel is influenced by the increase of the Reynolds number,
- Inside the TE outlets, any secondary structure is detected on the upstream face of the pedestals at the PS.
- The rotation affects a lot the flow field at the TE region by accelerating its velocity and disappearing the horse-shoe structures seen in stationary conditions results.
- The choice of the *SST k-w* model, even if it reproduces well the flow behaviour near and far the wall, it over-predicts the turbulence *Kinetic Energy (k)* which leads to the observed discrepancies at the inter-pedestals TE exit region.

Authors think that additional examination are required to explore the flow conditions at the suction side regions at the inter pedestal region, and for different turbulence models.

1.4 Acknowledgements:

The authors would like to express thanks to Drs: L. Bonanni, F. Maiolo and A. Pichi for the experimental help. Special gratefulness goes to Pr. A. Andreini for his numerical simulation support. As well, our acknowledgments go to Drs. A. Armellini and M. Pascotto of the University of Udine, Italy, for sharing the PIV velocities profiles.

Authors gratefully acknowledged the Italian research project PRIN, the funding of the Italian ministry for education, university and research (MIUR) for helping to achieve the reported work.

References:

[1] Thomas Hawksley Lecture. Adress by Captain H. Riall Sankey on Heat Engines to the Institution of Mechanical Engineersin November 1917.

[2] R. J. Hunt, The History of the Industrial Gas Turbine - Part 1: The First Fifty Years 1940-1990, idgtE, The Institution of Diesel and Gas Turbine Engineers, Bedford Heights, Manton Lane, Bedford MK41 7PH, publication: 582, 2011.

[3] J. C. Han , S. Dutta. and S. V. Ekkad., 2000, Gas turbine heat transfer and cooling technologies. Taylor & Francis, ISBN 156032841X, New York , NY 10001.

[4] E. Metzger, S. W. Haley, 1982, Heat transfer experiments and flow visualization for arrays of short pin fins, ASME Paper 82GT138.

[5] E. Metzger, R. A Berry, and J. P. Bronson., 1982, Developing heat transfer in rectangular ducts with staggered arrays of short pin fins. ASME journal of Heat Transfer, pp 104(1):700706.

[6] E. Metzger, W. B. Shepard, and S. W. Haley, 1986, Row resolved heat transfer variations in pinfin arrays including effects of nonuniform arrays and flow convergence. ASME Paper, 86GT132.

[7] Z. Wang,. Ireland. P. T, and Jones. T. V, 1993, Detailed heat transfer coefficient measurements and thermal analysis at engine conditions of a pedestal with fillet radii. (GT1993329).ASME Turbo Expo.

[8] Z. Wang., T. V. Jones., Ireland. P. T, and Kohler. S. T, 1994, Measurements of local heat transfer coefficient over the full surface of a bank of pedestals with fillet radii. GT1994307 .ASME TurboExpo.

[9] M. E. Taslim and T. Li, 1998, “Measurements of heat transfer coefficients in rib-roughened trailing-edge cavities with crossover jets,” ASME Paper NO-98GT-435,

[10] M. E. Taslim and A. Nongsaeng, 2011.“Experimental and numerical cross-over jet impingement in an airfoil trailing-edge cooling channel,” Journal of Turbomachinery, vol. 133, no. 4, Article ID 041009.

[11] J. J. Hwang. and C. C. Lui, 1999, Detailed heat transfer characteristic comparison in straight and 90° turned trapezoidal ducts with pinfin arrays. International Journal of Heat and Mass Transfer, V42 pp: 4005–4016.

[12] J. J. Hwang. and C. C. Lui, 2002, Measurements of endwall heat transfer and pressure drop in a pinfin wedge duct. International Journal of Heat and Mass Transfer, V:45 pp:877–889.

[13] B. Facchini., C. Carcasci, and L. Innocenti., 2003, Heat transfer and pressure drop evaluation in thin wedge shaped trailing edge. ASME GT200338197.

[14] S. W. Chang, T.-M. Liu, S. F. Chiou, and S. F. Chang, 2007,“High rotation number heat transfer of rotating trapezoidal duct with 45-° staggered ribs and bleeds from apical side wall,” in Proceedings of the ASME Turbo Expo, pp. 909–921, Montreal, Canada.

[15] A. P. Rallabandi, Y.-H.Liu, and J.-C. Han, 2010, “Heat transfer in trailing edge wedge-shaped pin-fin channels with slot ejection under high rotation numbers,” in Proceedings of the ASME Turbo Expo, pp. 369–380, Glasgow, UK.

[16] N. Kulasekharan and B. Prasad. 2008, Effect of coolant entry orientation on flow and heat transfer in the trailing region channels of a gas turbine vane. Proceedings of ASME Turbo Expo 2008: Power for Land, Sea and Air, GT2008-50951,.

[17] C. Bianchini, L. Bonanni, C. Carcasci, B. Facchini, and L. Tarchi. 2010, “Experimental survey on heat transfer in an internal channel of a trailing edge cooling system”.65 Associazione Termotecnica Italiana National Congress.

[18] C. Bianchini, B. Facchini, F. Simonetti, L. Tarchi, and S. Zecchi. 2010, Numerical and experimental investigation of turning flow effects on innovative pin fin arrangements for trailing edge cooling configurations. In Proceedings of ASME Turbo Expo 2010: Power for Land, Sea and Air, GT2010-23536.

[19] A. Armellini, L. Casarsa, and C. Mucignat, 2011, “Flow field analysis inside a gas turbine trailing edge cooling channel under static and rotating conditions,” International Journal ofHeat and Fluid Flow, vol. 32 (6), pp. 1147–1159.

[20] L. Bonanni, C. Carcasci, B. Facchini, and L. Tarchi. 2012, “Experimental survey on heat transfer in a trailing edge cooling System: effects of rotation in internal cooling ducts”. ASME Paper GT2012-69638.

[21] J. E. Hart, “Instability and secondary motion in a rotating channel flow,” Journal of Fluid Mechanics, vol. 45, pp. 341–351, 1970.

[22] C. G. Speziale, “Numerical study of viscous flow in rotating rectangular ducts,” Journal of Fluid Mechanics, vol. 122, pp. 251– 271, 1982.

[23] C. G. Speziale and S. Thangam, “Numerical study of secondary flows and roll-cell instabilities in rotating channel flow,” Journal of Fluid Mechanics, vol. 130, pp. 377–395, 1983.

[24] J.P. Johnston, R.M. Halleen, and D.K. Lezius, 1972. Effects of spanwise rotation on the structure of two dimensional fully developed turbulent channel flow, J. Fluid Mech., Vol. 56, pp. 533-557.

[25] H. Wu, Liu Y, Xu G, 2013, “Measurements of heat transfer and pressure in a trailing edge cavity of a turbine blade’. Chinese Journal of Aeronautics”, Vol 26(2), pp. 294–308.

[26] F. Coletti, M. Scialanga, and T. Arts, 2011, “Experimental investigation of conjugate heat transfer in a rib-roughened trailing edge channel with crossing jets,” Journal of Turbomachinery, vol. 134, no. 4, Article ID 041016.

[27] F. Coletti,1, D. Lo Jacono, I. Cresci, and T. Arts1, 2014, Turbulent flow in rib-roughened channel under the effect of Coriolis and rotational buoyancy forces, Journal of PHYSICS OF FLUIDS, Vol 26, 045111.

[28] E. E. Donahoo, A. K. Kulkarni, A. D. Belegundu, and C. Camci.2001, Determination of optimal row spacing for a staggered cross-pin array in a turbine blade cooling passage. Journal of Enhanced Heat Transfer, 8:41–53.

[29] A. Ooi, G. Iaccarino, P. A. Durbin, and M. Behnia, 2002, “Reynolds averaged simulation of flow and heat transfer in ribbed ducts,” International Journal of Heat and Fluid Flow, vol. 23, no. 6, pp. 750–757.

[30] D. D. Luo, C. W. Leung, T. L. Chan, and W. O. Wong, 2005, “Simulation of turbulent flow and forced convection in a triangular duct with internal ribbed surfaces,” Numerical Heat Transfer A, vol. 48, no. 5, pp. 447–459.

[31] A. K. Viswanathan and D. K. Tafti, 2006, “Detached eddy simulation of turbulent flow and heat transfer in a two-pass internal cooling duct,” International Journal of Heat and Fluid Flow, vol. 27, no. 1, pp. 1–20,.

[32] S. Spring, Y. Xing, and B. Weigand, 2012, “An experimental and numerical study of heat transfer from arrays of impinging jets with surface ribs,”Journal of Heat Transfer, vol.134 , no.8 , Article ID 082201.

[33] A. K. Saha and S. Acharya, 2007 ,“Turbulent heat transfer in ribbed coolant passages of different aspect ratios: parametric effects,” Journal of Heat Transfer, vol. 129, no. 4, pp. 449–463.

[35] P. D’Agaro and G. Comini.2008, Thermal-performance evaluation of coolant passages with staggered arrays of pin fins. International journal of Heat and Mass Transfer, 44:815–825.

[34] G. Delibra, D. Borello, K. Hanjalic, and F. Rispoli. 2009, URANS of flow and endwall heat transfer in a pinned passage relevant to gas-turbine blade cooling. International Journal of Heat and Mass Transfer, no 30, pp: 549–560.

[35] E. Di Carmine, B. Facchini, and L. Mangani.2008, Investigation of innovative trailing edge cooling configurations with enlarged pedestals and square or semi-circular ribs. Part II - numerical results. Proceedings of ASME Turbo Expo 2008: Power for Land, Sea and Air, GT2008-51048.

[36] M. Schuler, H. Dreher, S. O. Neumann, B.Weigand, and M. Elfert. 2010, Numerical predictions of the effect of rotation on fluid flow and heat transfer in an engine-similar two-pass internal cooling

channel with smooth and ribbed walls. In Proceedings of ASME Turbo Expo 2010: Power for Land, Sea and Air, GT2010-22870.

[37] C. Prakash and R. Zerkle.1995, Prediction of turbulent flow and heat transfer in a ribbed rectangular duct with and without rotation.Journal of Turbomachinery, (117).

[38] K. Tafti and A. M. Elyyan.2010, Investigation of Coriolis forces effect of flow structure and heat transfer distribution in a rotating dimpled channel. Proceedings of ASME Turbo Expo 2010: Power for Land, Sea and Air, GT2010-22657.

[39] A. K. Saha and S. Acharya, 2005, "Unsteady RANS simulation of turbulent flow and heat transfer in ribbed coolant passages of different aspect ratios," International Journal of Heat and Mass Transfer, vol. 48, no. 23-24, pp. 4704–4725.

[40] L. Andrei, A. Andreini, L. Bonanni, and B. Facchini. 2010, "Heat transfer in internal channel of a blade: effects of rotation in a trailing edge cooling system". *10th International Symposium on Experimental Computational Aerothermodynamics of Internal Flows*, (ISAIF10-99).

[41] M. Pascotto, A. Armellini, L. Casarsa, C. Mucignat, and P. Giannattasio, 2013, Effects of Rotation at Different Channel Orientations on the Flow Field inside a Trailing Edge Internal Cooling Channel, International Journal of Rotating Machinery Vol 2013, Article ID 765142.

[42] A. Beniaiche, A. Ghenaiet, C. Carcasci, M. Pievarolli and B. Facchini, 2015, Experimental study of a cooling scheme for a turbine blade trailing edge, Proc. IMechE Part A: Journal of Power and Energy, Vol. 229 no 8, pp: 832-848.

[43] A. Beniaiche, A. Ghenaiet, B. Facchini , 2016, Experimental and numerical investigations of internal heat transfer in an innovative trailing edge blade cooling system: stationary and rotation effects, part 1: Experimental results, Journal of heat and Mass transfer, Vol 52 ,N°6, 15 pages.

[44] A. Beniaiche, A. Ghenaiet, B. Facchini , 2016, Experimental and numerical investigations of internal heat transfer in an innovative trailing edge blade cooling system: stationary and rotation effects, part 2: numerical results, Journal of heat and Mass transfer, Vol 52 ,N°6, 15 pages.

[45] I. B. Celik,U. Ghia, P. J. Roache, C. J. Freitas, H. Coleman, and P.E. Raad, 2008, "Procedure for estimation and reporting of uncertainty due to discretization in CFD applications," Journal of Fluids Engineering, vol. 130, no. 7, pp. 0780011–0780014.

[46] L. Richardson and A. Gaunt, 1927, "The deferred approach to the limit.Part I. single lattice. Part II. interpenetrating lattices," Philosophical Transactions of the Royal Society of London A, vol. 226, no. 636–646, pp. 299–361.

[47] P. J. Roache, 1994, "Perspective: a method for uniform reporting of grid refinement studies," Journal of Fluids Engineering, Transactions of the ASME, vol. 116, no. 3, pp. 405–413.

[48] P. J. Roache, 2003, “Conservatism of the grid convergence index in finite volume computations on steady-state fluid flow and heat transfer,” Journal of Fluids Engineering, Transactions of the ASME, vol. 125, no. 4, pp. 731–732.

[49] D. R. H. et al, 2000, Detailed flow and heat transfer coefficient measurements in a model of an internal cooling geometry employing orthogonal interesting channels, ASME TurboExpo, May 8-11 Germany, Munich, Germany.

[50] R.Yu, Y.Xu, 2012, “Uncertainty Analyses and Its Application to Turbulent Heat Transfer Measurements”, Advances in Condensed Matter Physics Journal, Vol. 2012, Article ID 898104.

List of tables:

The inlet section of a high aspect ratio	AR=7.25
Hydraulic diameter (D_h)	58.18 mm
Gonverging wedge shaped duct angle	$\alpha = 10°$
Initial height (H1)	33 mm
P_x	75 mm
Pedestal's length	84 mm
Pedestal's extreme diameter	12 mm
Ribs inclination	+ 60°
The rotation axis z position/inlet section	174 mm
The operating conditions	Open tip - Re = 10000 – 40000 - Ro = 0 – 0.23
	Closed tip: Re = 10000 – 40000 Ro = 0 – 0.23
Validations	PIV technique: aerodynamic data TLC technique: Thermal data

Table 1: Characteristics and operating conditions of the present study.

Planes	**z position (mm)**
A xy	*14.55*
B xy	*-14.55*
xy	*0*

Table 2: Positions of *xy planes* in the *z* direction.

Planes	**Position (mm)**
xz1	*y = -150*
xz2	*y = -165*
xz3	*y = -180*
yz	*x = -69.8*

Table 3: Positions of *xz*and*yz planes*.

		N.10^6	y^+_{max}	y^+_{avg}
Case: +60° Ribbed geometry				
Coarse	Present study	2.04	2.02	0.61
Intermediate	Present study	4.48	1.77	0.44
Fine	Present study	9.8	1.28	0.35

Table 4: Comparison of the obtained results of the y^+_{max} and y^+_{avg} for the different mesh sizes, Ribbed surfaces.

.

List of figures:

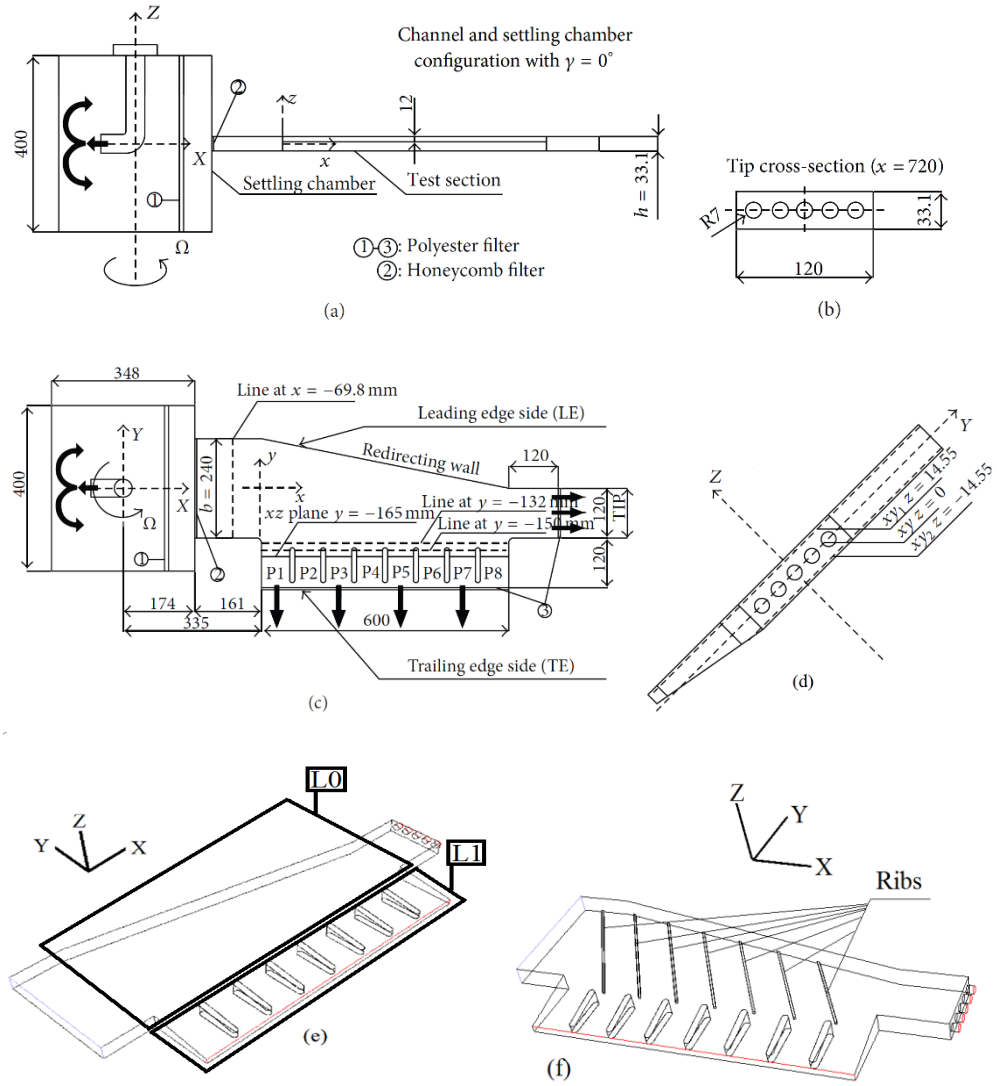

Figure 1: Schematic (a–d) and 3-D view (e, f) of the test section investigated in the present study.

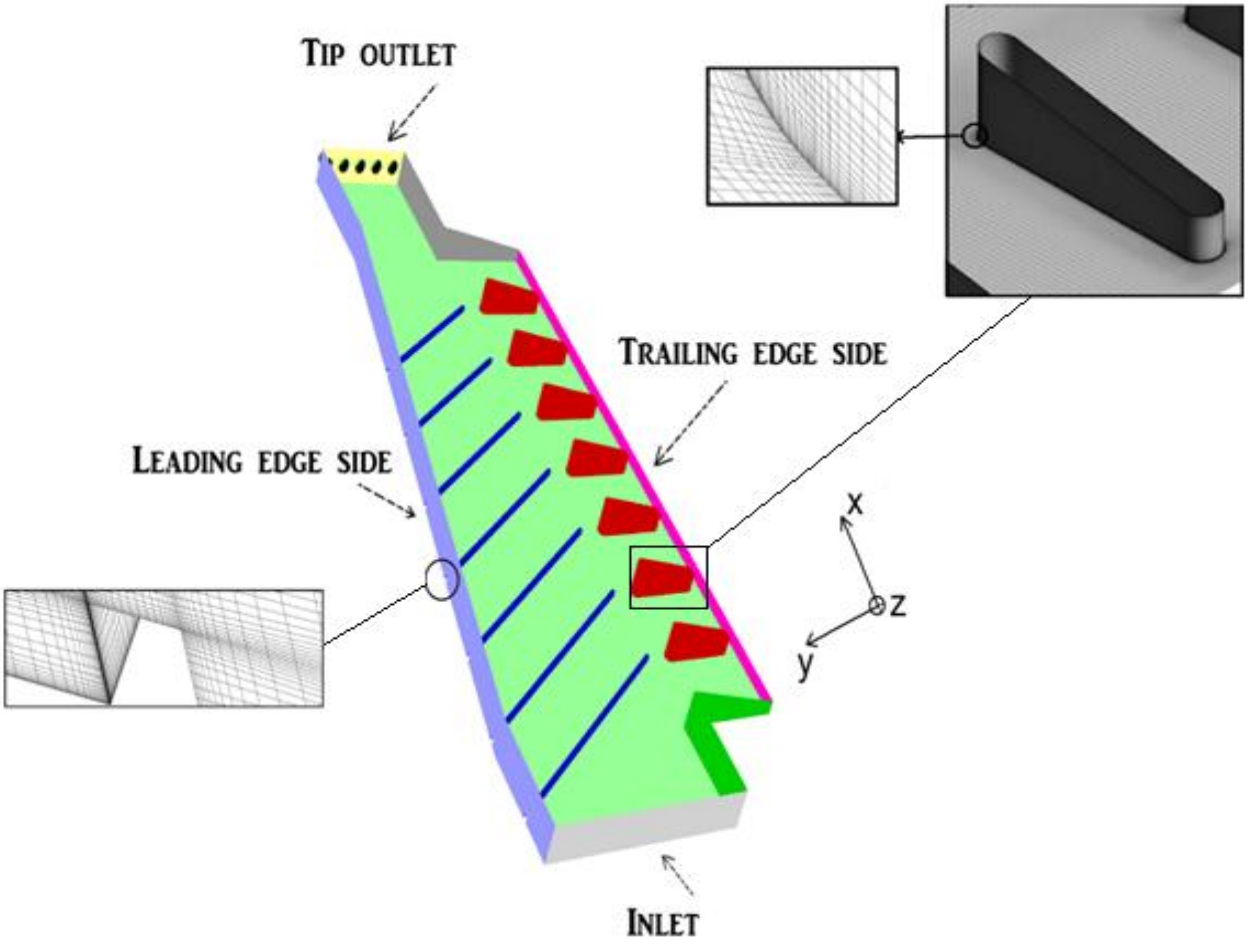

Figure 2 : Details of the studied mesh.

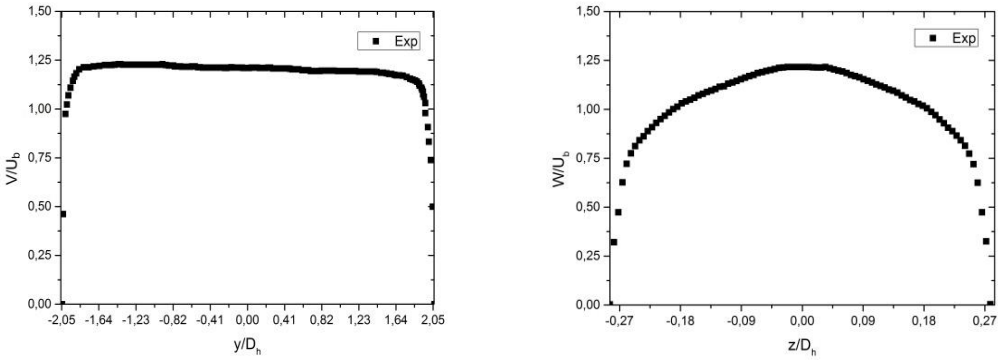

(a) v_{meanY} (y/D_h). (b)v_{meanX} (z/D_h).

Figure 3: Experimental [27] and numerical V/Ub velocity profiles at the channel inlet, x= −69.8 mm, Ro=0.

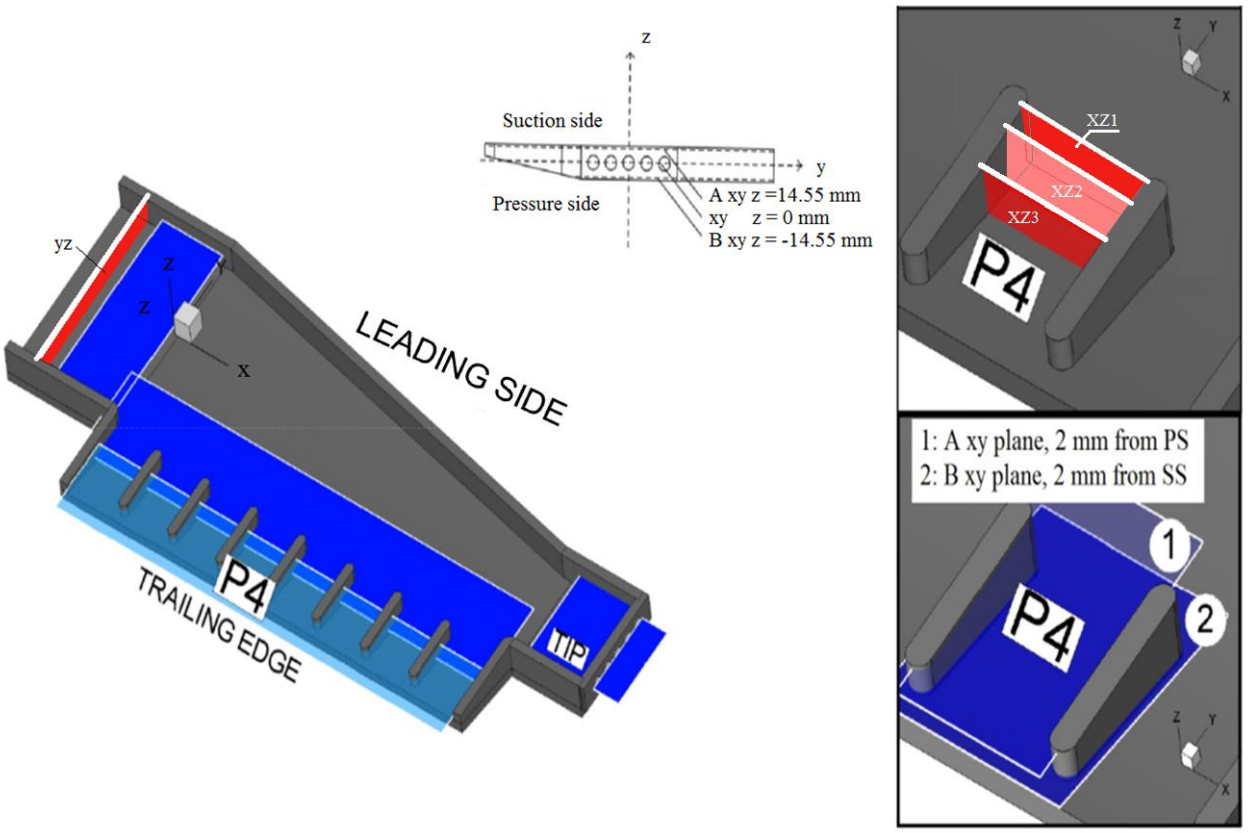

Figure 4 : Position of the different planes.

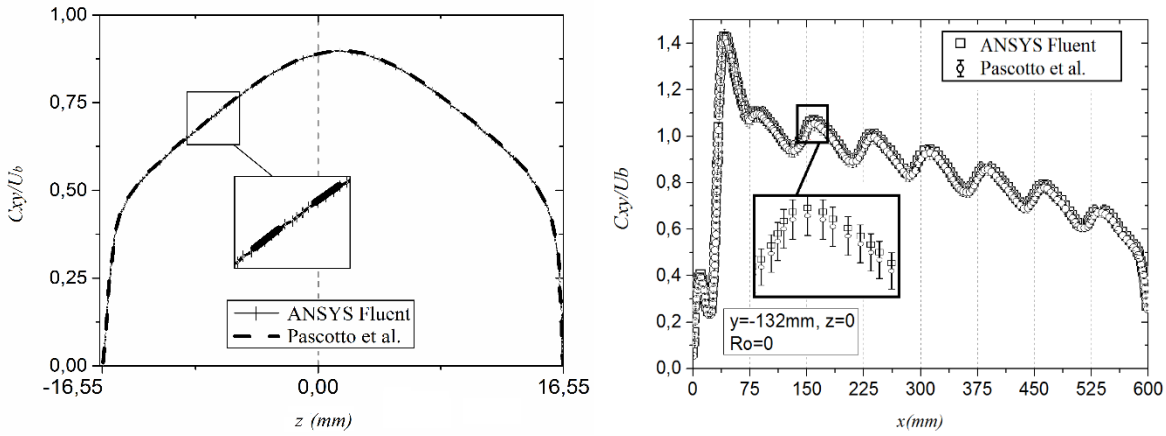

(b)

Figure 5 : Comparison results of the present study and [41]of the GCI error band from the mesh sensitivity analysis for the profiles of the velocity magnitude in plane xy,$Cxy = (U^2+V^2)^{0.5}$, extracted at $y = -132$ mm, (a) plane: $x = 300$mm, $y = -132$ mm, (b) plane: $z = 0$mm, respectively. Smooth surface, Open tip. [44]

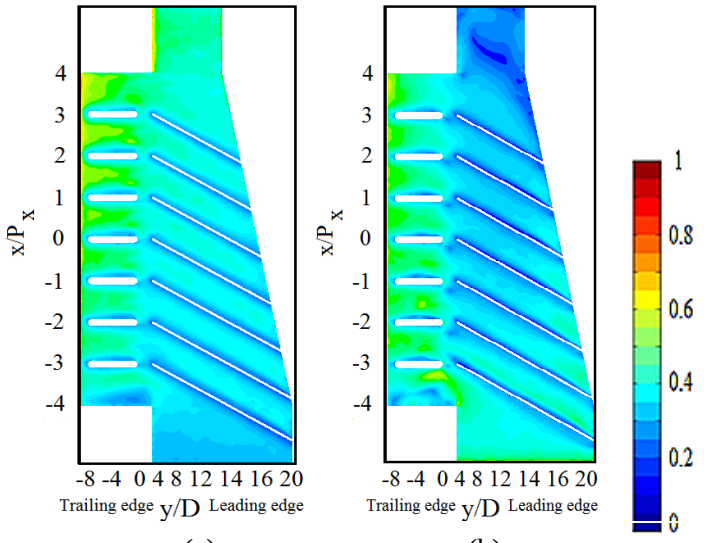

(a) (b)

Figure 6 : 2D y^+ maps distribution over the heated surface for Re=20000, Ro=0 : (a) Smooth surface open tip (b) Smooth surface closed tip (c) Ribs +60 ° open tip (d) Ribs +60 ° closed tip.

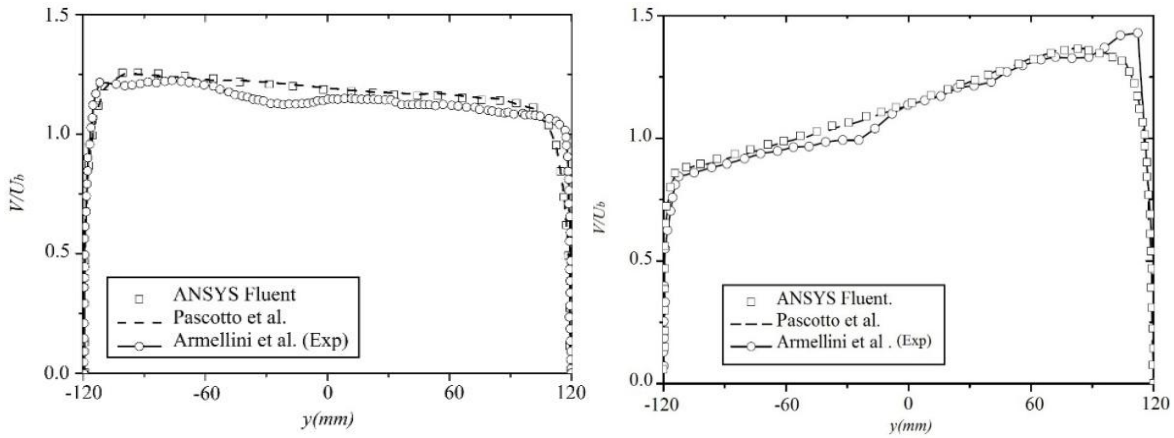

(a) (b)

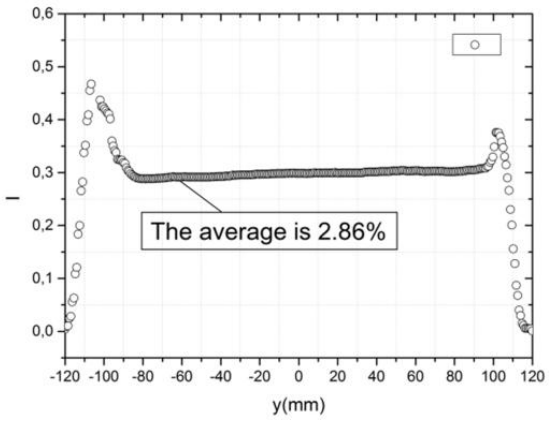

(c)

Figure 7 : Experimental [19] and numerical V/U_bvelocity profiles at the channel inlet, Smooth surface, Open tip, $x = -69.8$ mm, $y = z = 0$: (a) Ro = 0, (b) Ro =0.23, (c) Turbulence Intensity I variation along $x = -69.8$ mm, $y = z = 0$, Open tip.

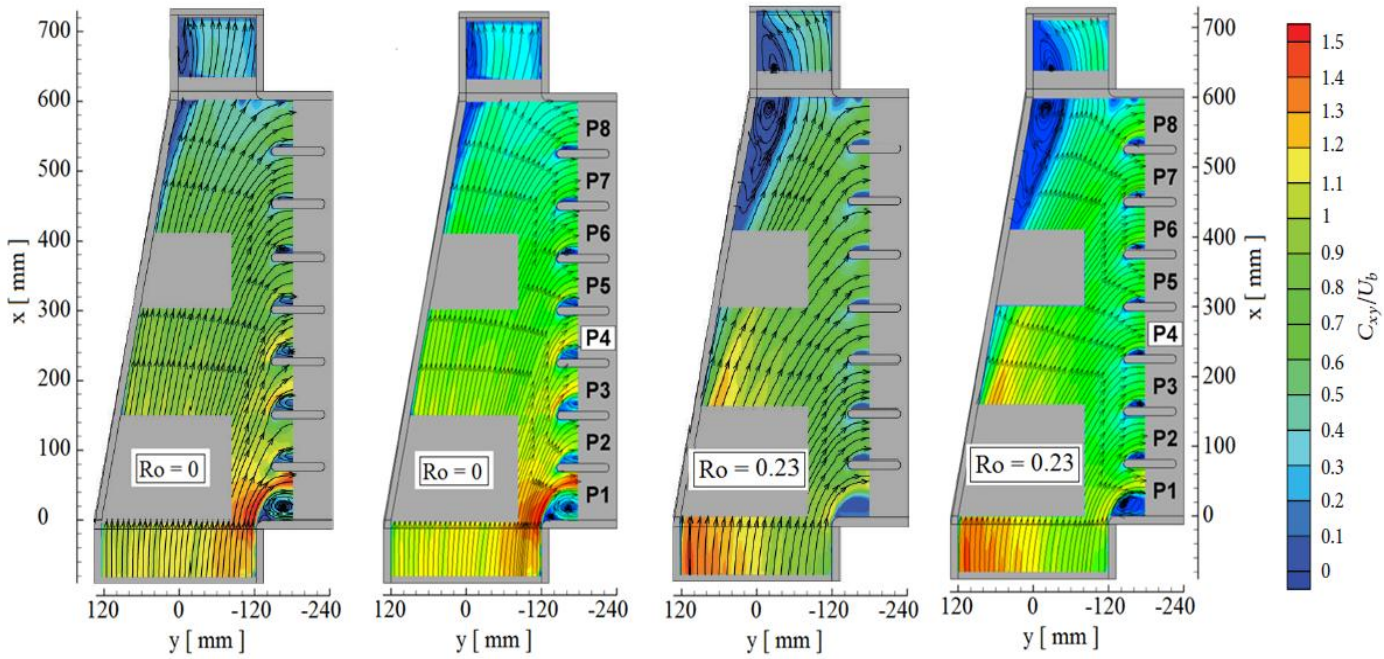

(a) (b) (c) (d)

Figure 8 : The C_{xz}/U_bVelocity profile distribution comparison of, Open tip, *xy* plane at z = 0 mm, Re=20000, Ro=0,(a,c) Experimental PIV data [41] (b,d) Present CFD prediction. (a,b) Stationary (c,d) Rotating.

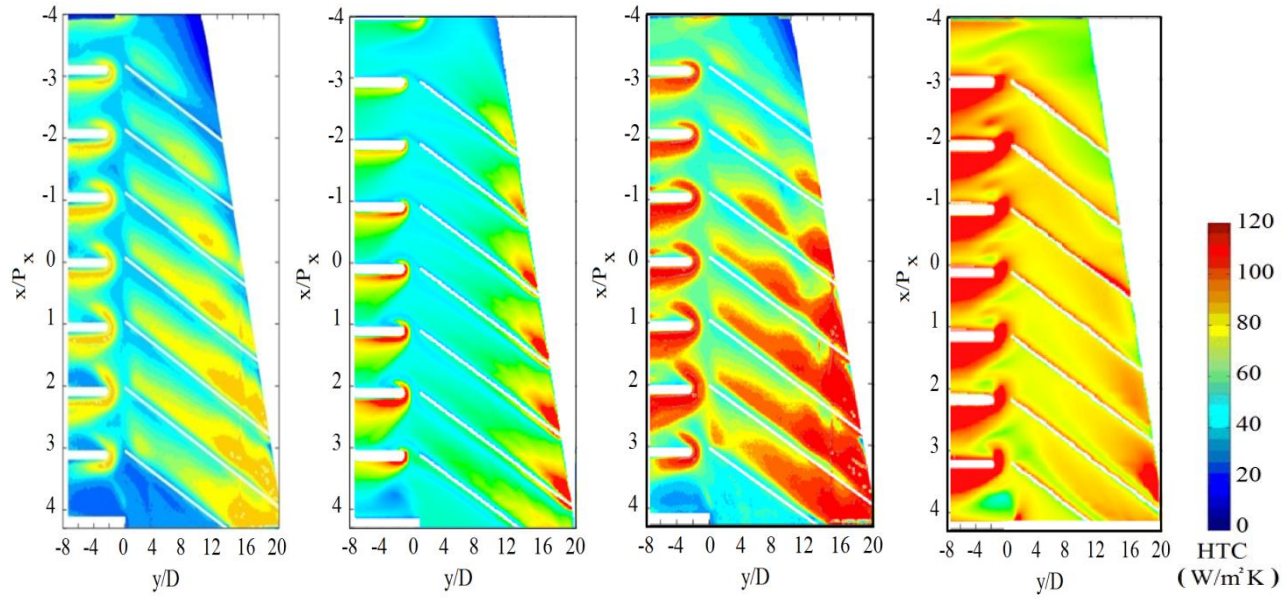

(a) (b) (c) (d)

Figure 9: 2D HTC maps distribution, Ribs +60°, closed tip, Ro = 0.23, (a,b) Re= 20000, (c,d) Re= 40000, (a,c) Experimental (b,d) CFD.

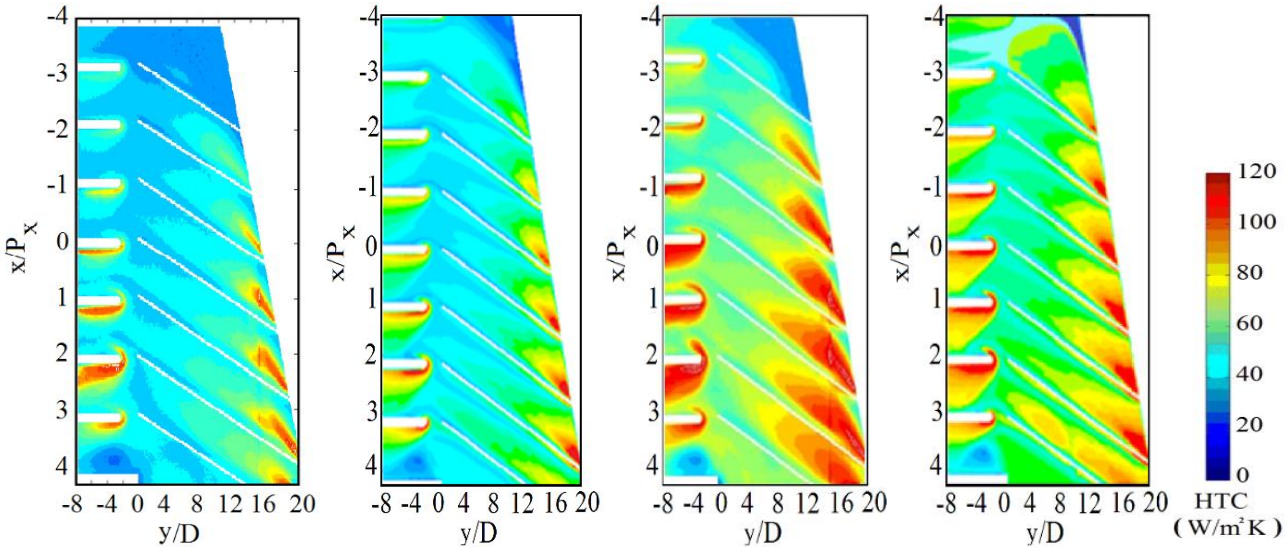

(a) (b) (c) (d)

Figure 10 : 2D HTC maps distribution (TLC), Ribs +60°, closed tip, Ro = 0, (a,b) Re= 20000, (c,d) Re= 40000, (a,c) Experimental [42] (b,d) CFD.

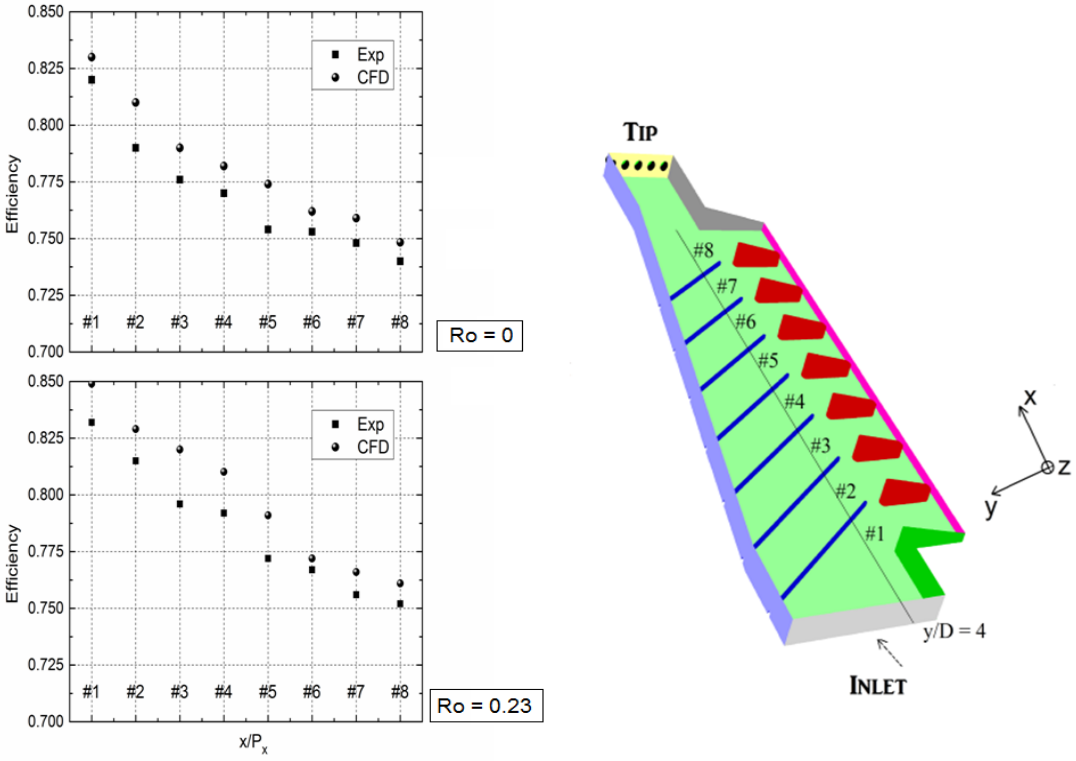

Figure 11: The coolant temperature potential, Open tip, y/D = - 4, Re= 20000, Ro = 0-0.23, Smooth geometry: Experimental and CFD results.

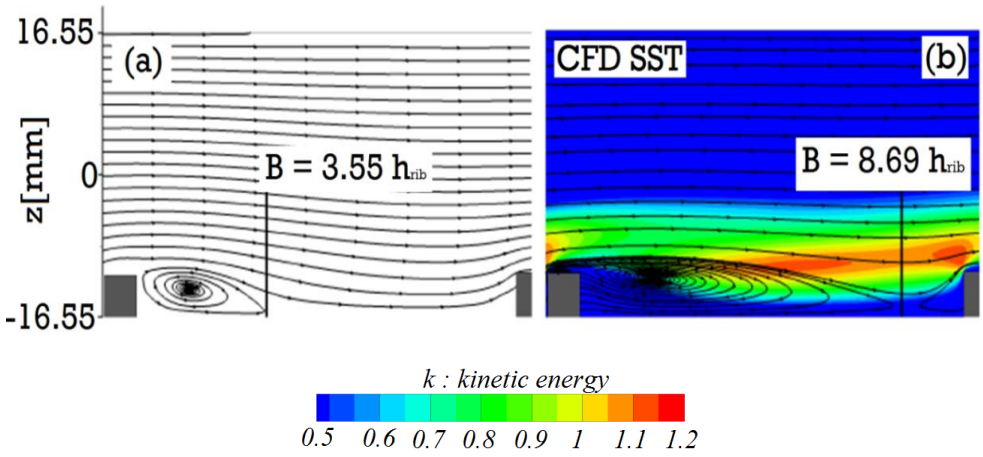

Figure 127: The stream-tracers distribution of the normalized turbulence kinetic energy *k* , Experimental PIV [23] (a) vs CFD (b) in the 3rd to 4th ribs passage at the xz, y = 0 mm plane.

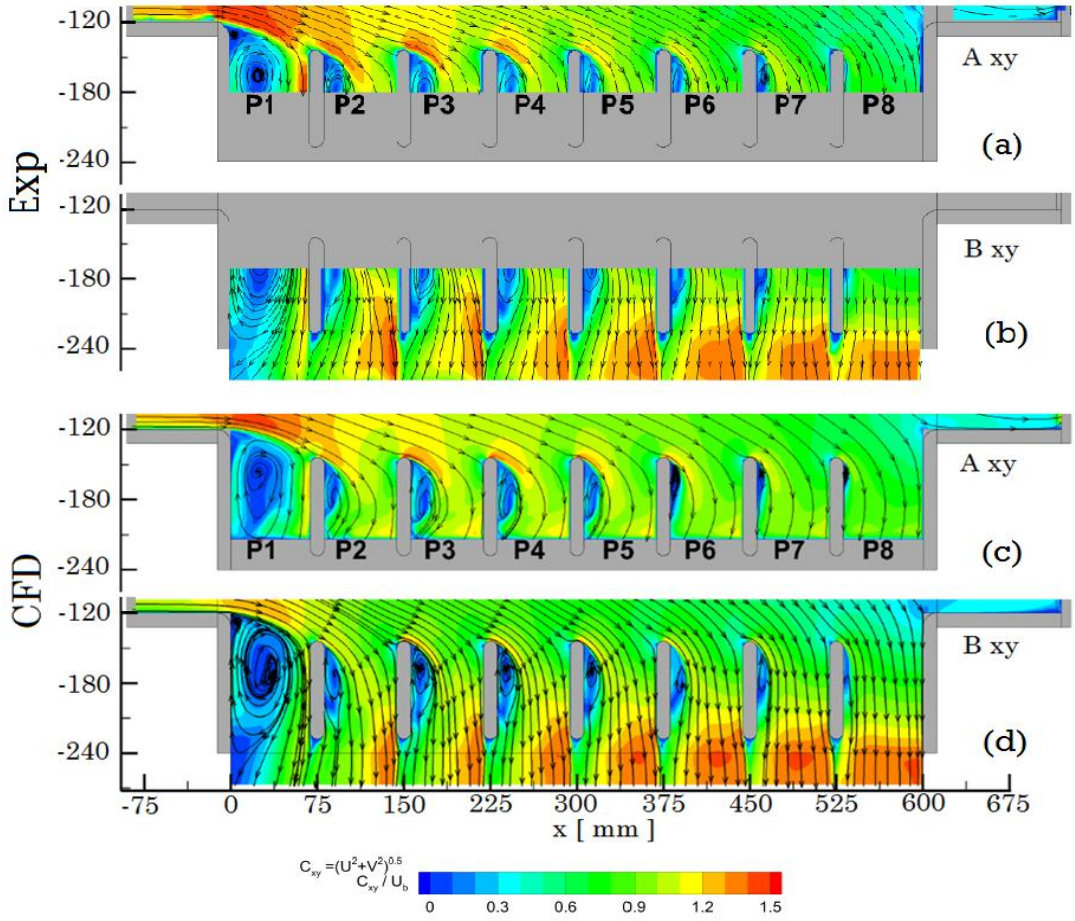

Figure 13: Time averaged stream-tracers and contour plots of the in plane velocity modulus C_{xy} Experimental PIV [19] (a,b) *vs* CFD (c,d), in the Axy (a,c) and B xy (b,d) planes, for Re = 20000, open tip configuration.

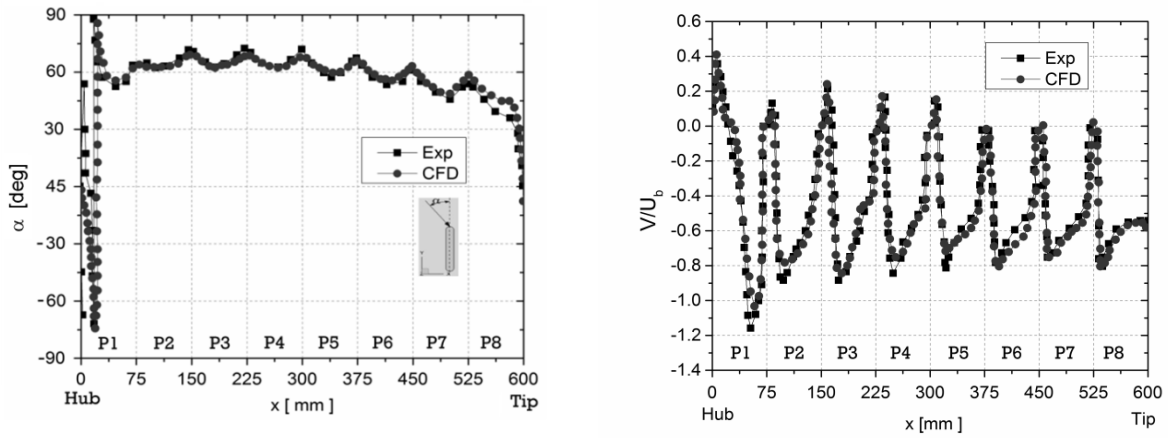

(a) (b)

Figure 8: Experimental [19] vs CFD flow characteristics: (a) angle of attack α (b) time averaged velocities V/U profiles at line y =-132 mm, Re = 20000, Ro =0.00, open tip configuration.

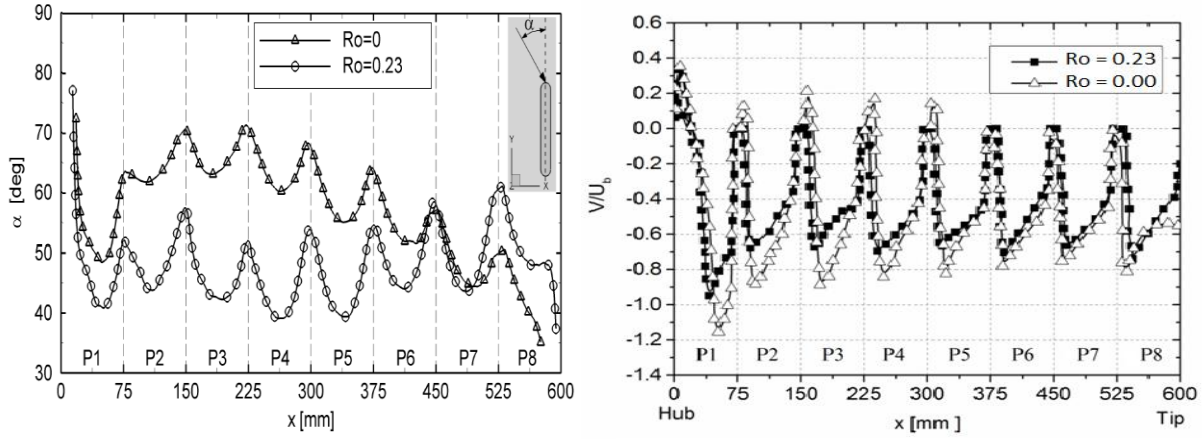

(a) (b)

Figure 15: Experimental data [19] vs CFD data flow features: (a) angle of attack α (b) Profiles of time averaged velocities V/U_b , at line y =-132 mm, Re = 20000, Ro =0-0.23, open tip configuration.

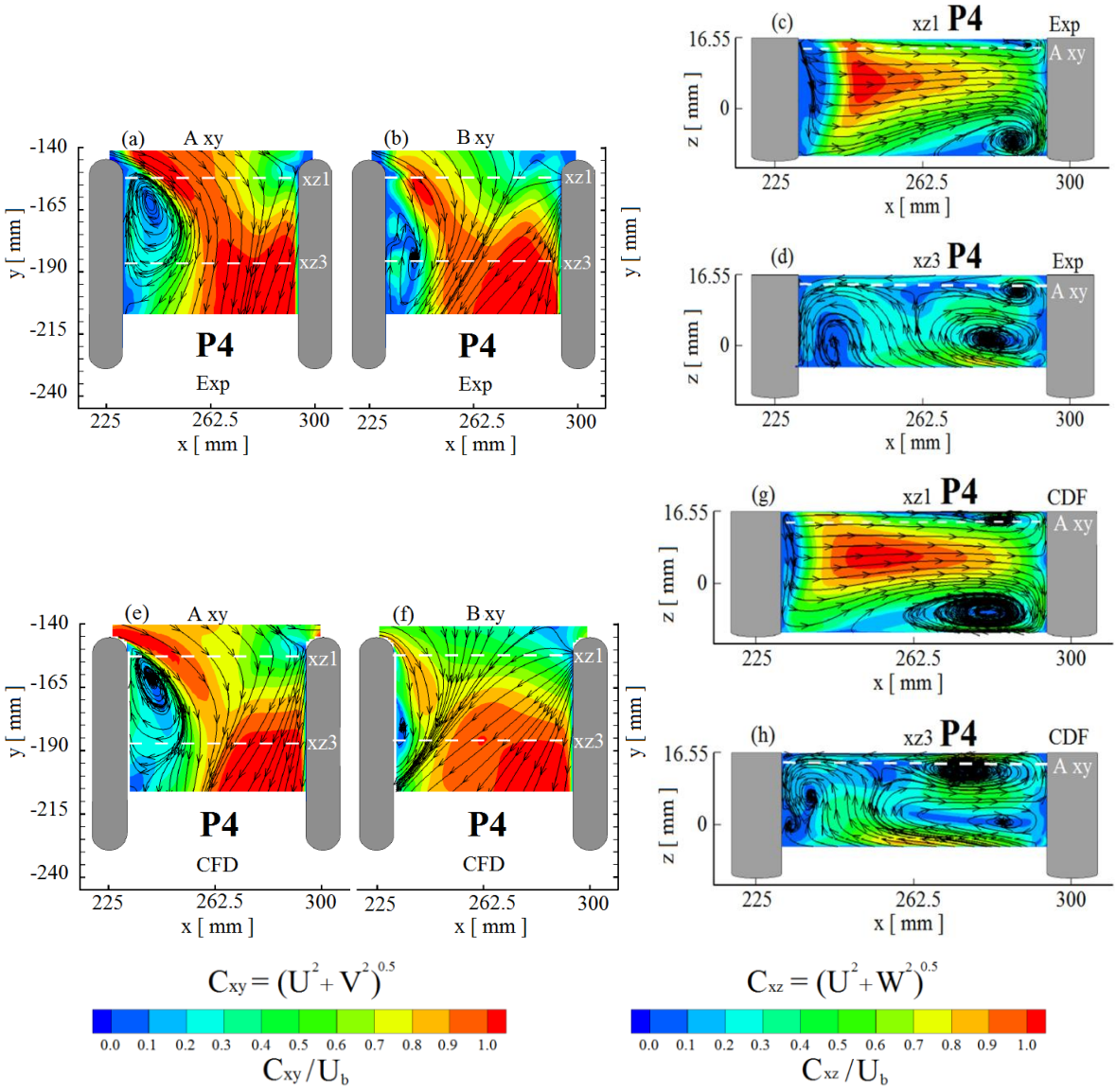

Figure 96: Illustration of flow field within the inter-pedestal passage P4: (a, b, c) Experimental PIV [19] (d, e,f) CFD results. Ro = 0, Re = 20000, Open tip configuration.

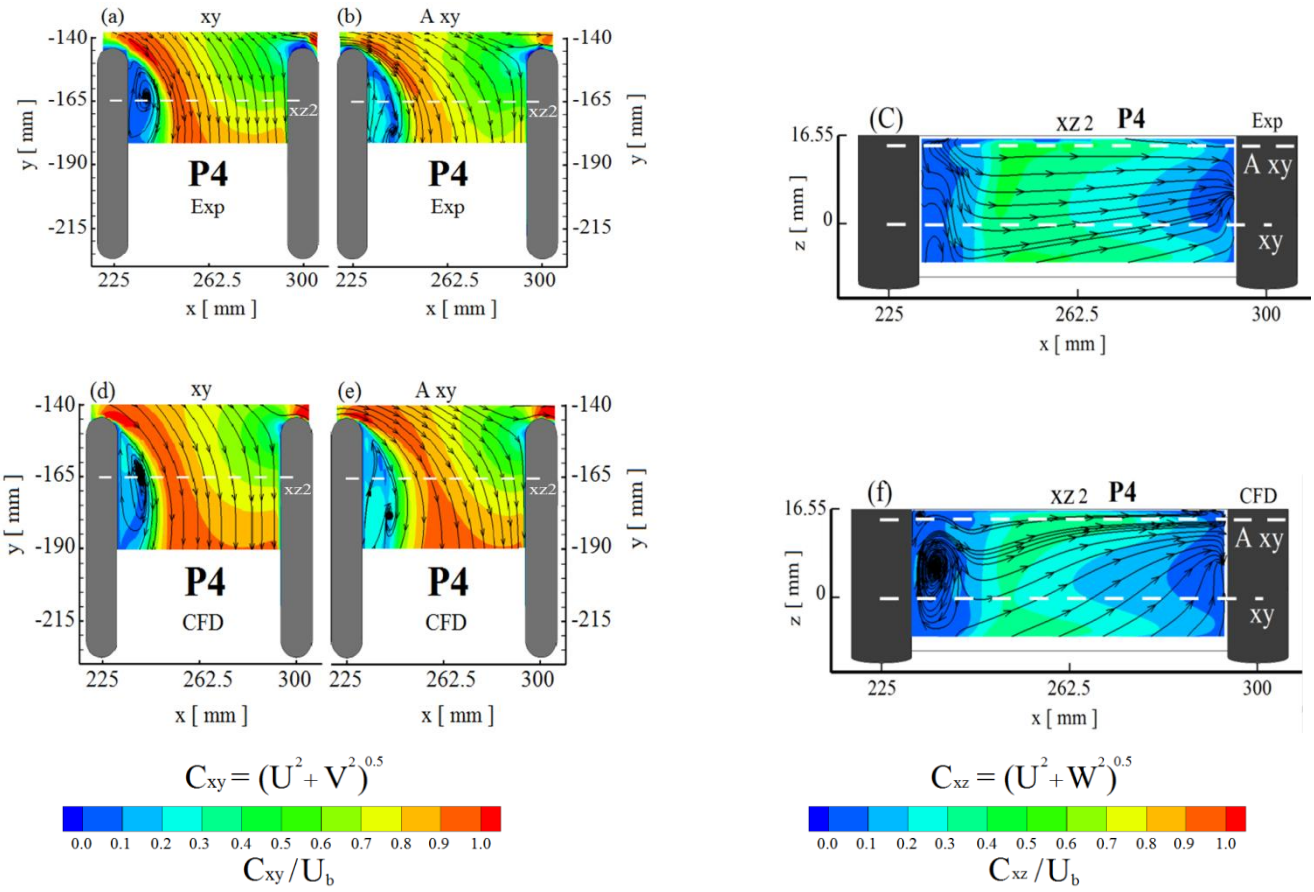

Figure 17: Illustration of flow field within the inter-pedestal passage P4 at: (a,d) plane : xy, z = 0 mm, (b,e) plane : A xy, z = 14.55 mm, (c,f) plane : xz 1, y = -150 mm, (a, b, c) Experimental PIV, (d, e,f) CFD results, Re = 20000, Ro = 0.23, Open tip configuration.

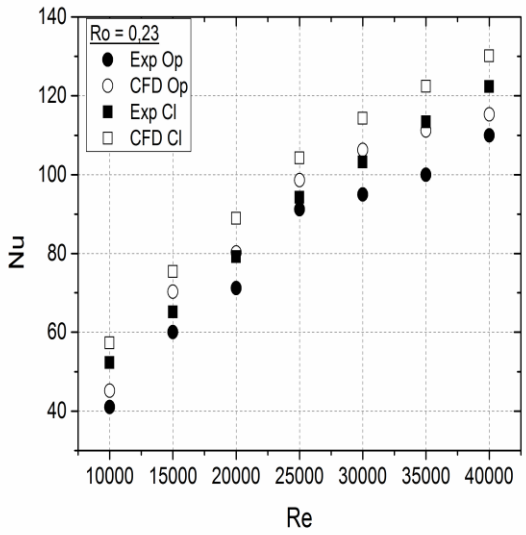

Figure 18: P4 region's Averaged Nusselt number : Experimental vs CFD results, for +60° ribbed surface, Open and closed tip configurations, Re =10000-40000, Ro = 0.23.